Radboud Repository

Radboud University Nijmegen

PDF hosted at the Radboud Repository of the Radboud University Nijmegen

The following full text is a publisher's version.

For additional information about this publication click this link.
http://hdl.handle.net/2066/83529

Please be advised that this information was generated on 2017-12-06 and may be subject to change.

Coherent and spontaneous Rayleigh-Brillouin scattering in atomic and molecular gases and gas mixtures

M. O. Vieitez,[1] E. J. van Duijn,[1] W. Ubachs,[1] B. Witschas,[2] A. Meijer,[3] A. S. de Wijn,[3] N. J. Dam,[3] and W. van de Water[4,*]

[1]*Laser Centre, Vrije Universiteit, De Boelelaan 1081, NL-1081 HV Amsterdam, The Netherlands*
[2]*Deutsches Zentrum für Luft- und Raumfahrt DLR, Institut für Physik der Atmosphäre, Oberpfaffenhofen, Germany*
[3]*Institute of Molecules and Materials, Applied Molecular Physics, Radboud University, NL-6500 HC Nijmegen, The Netherlands*
[4]*Physics Department, Eindhoven University of Technology, Postbus 513, NL-5600 MB Eindhoven, The Netherlands*

We study Rayleigh-Brillouin scattering in gases of N_2, O_2, and SF_6 molecules, Kr atoms, and He-Xe and He-CO_2 mixtures at pressures ranging from 1 to 3 bar and using two different experimental setups. In one setup, we measure spectra of light scattered by thermal density fluctuations (spontaneous Rayleigh-Brillouin scattering); in the second setup density waves are induced in the overlap region of two counterpropagating laser beams (coherent Rayleigh-Brillouin scattering). We compare measured spectra to the Tenti models and to a recent model for mixtures. We find new values of the bulk viscosity, which is a parameter in line-shape models that allows for internal degrees of freedom. Both experiments agree on the value of the bulk viscosity. Our results indicate a need for new line-shape models for mixtures of molecules with internal degrees of freedom.

PACS number(s): 42.65.Es, 42.68.Ca, 42.68.Wt

I. INTRODUCTION

The physical phenomenon of light scattering by small particles of size smaller than the wavelength of the incident light has been understood in the framework of electromagnetism since the pivotal studies by Rayleigh [1] more than a century ago. Fluctuations in the dielectric constant of the gas, at the deepest level associated with the particle nature of gases, are the cause of light scattering. In Rayleigh's theory, the scattering cross section is directly connected to the index of refraction of the gaseous medium. Later, the polarization and depolarization properties in these scattering processes were investigated [2]. Initially these scattering phenomena were considered to be elastic until Raman showed that internal degrees of freedom of the molecular scattering center affect the spectral distribution of the scattered light [3]. The spectral line shape is not only determined by such single-molecule properties, but also by collective effects such as density fluctuations in the gas, which give rise to the pronounced Brillouin sidebands of the central elastic scattering peak. These acoustic modes become more pronounced at higher densities and the scattering phenomenon is known as Rayleigh-Brillouin scattering. The study of the exact Rayleigh-Brillouin spectral line shape is of practical relevance since it provides information on the velocity, density, and temperature of the illuminated gas samples.

Methods of kinetic theory have been successfully used for the prediction of spectral line-shapes of Rayleigh-Brillouin scattering [4,5]. However, as light scattering experiments and the analysis of spectral data become more and more precise, there is an urgent need to test the precision of line-shape models. These line-shape models are of key importance for the quantitative interpretation of lidar experiments, such as the satellite-based lidar study ADM-Aeolus planned by the European Space Agency (ESA) [6]. Kinetic line-shape models use macroscopic transport coefficients, such as the viscosity η, the bulk viscosity η_b, the heat conductivity λ, and the heat capacity c_{int} of the internal degrees of freedom of the gas, to model the microscopic collision integral. Most kinetic models are for single-component gases only. Air, on the other hand, is a gas mixture, and may also contain significant amounts of water vapor and CO_2. A model for the spectral line shape of light scattered in mixtures of gases was described recently, but has not yet been thoroughly tested [7,8].

Let us now briefly summarize earlier experiments on Rayleigh-Brillouin scattering. Rayleigh-Brillouin scattering in gases was first explored in the 1960s using narrow-band lasers and Fabry-Perot interferometers, which provide the frequency resolution needed to observe the Brillouin doublet due to scattering off thermal sound. Greytak and Benedek [9] used a frequency-stabilized HeNe laser (632.8 nm) delivering 0.6 mW and investigated several gases (Ar, Xe, N_2, CO_2, CH_4) at atmospheric pressure. They obtained spectra at scattering angles $\theta = 10.6°$ and $\theta = 169.4°$ using two different Fabry-Perot spectrometers, with 28-MHz and 205-MHz instrumental resolution, respectively. Hara, May, and Knaap [10] investigated the Rayleigh-Brillouin spectrum of the three isotopic variants of molecular hydrogen (H_2, HD, and D_2) at a scattering angle of $\theta = 90°$. They used a HeNe laser and a pressure-scanned parallel-plate Fabry Perot with a finesse of 50; its free spectral range (FSR) varied from 15 GHz for the H_2 experiments to 10 GHz for the D_2 and HD experiments. Sandoval and Armstrong [11] studied Rayleigh-Brillouin scattering in N_2 at a range of pressures (1–661 Torr) using a frequency-stabilized HeNe laser at a scattering angle of $\theta = 15°$. The instrument width of the piezoelectrically scanned Fabry-Perot spectrometer was 40 MHz. Using the kinetic model by Sugawara and Yip [12], they determined relaxation rates in a least-squares procedure. At near-atmospheric pressures they find $\eta_b \approx 3\eta$.

Lao, Schoen, and Chu [13,14] investigated Rayleigh-Brillouin scattering in a number of gases: CO_2, N_2, C_2F_6, C_2H_6 and a He-Kr mixture. A single-mode Ar-ion laser at 514.5 nm with a power up to 500 mW was used; scattering angles were varied, covering 90° and 60° for most cases. The Fabry-Perot spectrometer employed had an FSR of 2 GHz, with a 31 MHz

*W.v.d.Water@tue.nl

instrumental resolution. The measured spectra were analyzed with a hydrodynamic line-shape model, while the Tenti S6 model was compared to CO_2 and N_2 spectra. The bulk viscosities used ($\eta_b = 2.2 \times 10^{-6}$ and 1.28×10^{-5} kgm^{-1}s^{-1}, respectively) were computed from known rotational relaxation rates. It was concluded that, for CO_2, vibrational relaxation had no effect, a circumstance that was rediscovered later by Pan *et al.* [15].

Ghaem-Maghami and May [16,17] investigated the Rayleigh-Brillouin spectrum in both the kinetic and hydrodynamic regime of the noble gases He, Ne, and Ar. They found that, in the kinetic regime, the spectra can be parametrized to the 3% accuracy level with the dimensionless frequency and wavelength x and y, respectively [Eqs. (2) and (1)]. This is expected because noble gas atoms resemble hard spheres, for which the x and y parameters completely determine the spectrum.

Experiments on binary gas mixtures of noble gases and mixtures of He with H_2 and D_2 were done by Letamendia *et al.* [18,19]. They use a single-mode Ar-ion laser operating at 514.5 nm with a power of 800 mW, and a confocal (piezoelectrically scanned) Fabry-Perot spectrometer with a finesse of 50. The overall frequency resolution was 20 MHz. The scattering angles were varied between 30° and 150°. The results were compared to hydrodynamic and kinetic line-shape models.

Coherent Rayleigh-Brillouin scattering was first proposed by She *et al.* [20,21]. Grinstead and Barker [22] experimentally demonstrated coherent Rayleigh-Brillouin scattering in the collisionless limit, whereas Pan *et al.* performed measurements in the kinetic regime [23,24]. Data obtained in rare gases as well as in atmospheric gases at room temperature and various pressures were presented. Coherent Rayleigh-Brillouin scattering has been used for temperature measurements in low-density gases [25] as well as in flames [26]. In the latter case, it was shown that, by modeling the flame gas as a mixture of the dominant components (N_2, H, O, CO), the line shape in the collisionless regime is only weakly sensitive to the exact gas composition. Recent developments of the technique include the use of optical gratings formed by pump beams with different frequencies to modify the velocity distribution of molecules [27,28], and the theoretical exploitation of the high-intensity regime [29,30].

In this article we discuss experiments on N_2, O_2, SF_6, Kr, and He-Xe and He-CO_2 mixtures. The experiments were done in two completely different experimental arrangements. In the first one, we study scattering at 90° by spontaneous density fluctuations in a cell at a range of pressures. In the other arrangement, the density waves are induced by electrostrictive forces in the overlap region of two crossed laser beams. This arrangement, coherent Rayleigh-Brillouin scattering, which was recently explored by Pan *et al.* [23,24], has the advantage that the scattered light inherits the coherence properties of the density wave, and is concentrated in a beam, rather than being distributed over a 4π solid angle as in the spontaneous arrangement. The gain in intensity is so large that an entire spectrum may be obtained in a single laser shot. On the other hand, long integration times are needed in our spontaneous experiments. The advantage of the coherent arrangement is the insensitivity to stray reflected light, which presents a challenge

in the spontaneous arrangement. However, while the statistical error of the spontaneous experiment is due to photon collection statistics, mode fluctuations of the pump laser that makes the standing wave field are currently limiting the precision of the coherent Rayleigh-Brillouin scattering experiments.

All line-shape models use known values of the transport coefficients to parametrize the collision integral in the linearized Boltzmann equation. Most values are well established but, at the GHz frequencies of our experiments, the bulk viscosity η_b is poorly known. The bulk viscosity quantifies the relaxation of excited internal degrees of freedom due to molecular collisions. We will argue that the excellent signal-to-noise ratio of our experiments allows us to both determine a value for the bulk viscosity and establish the accuracy of line-shape models.

In Sec. II we discuss kinetic models for the spectral line shape in spontaneous and coherent Rayleigh-Brillouin scattering, while the nature of the bulk viscosity is discussed in Sec. IV. The two experimental techniques used in this work are briefly described in Secs. V A and V B, respectively. Results for the two experiments are described in Sec. VII.

II. LINE-SHAPE MODELS

Rayleigh-Brillouin scattering in gases originates from density fluctuations. These density fluctuations can either arise spontaneously in thermal equilibrium, or they can be induced deliberately in the coherent scattering arrangement. Let us call the incident- and scattered-light wave vectors $\boldsymbol{k}_p$ and $\boldsymbol{k}_s$, respectively. A key parameter is the ratio y of the scattering wavelength $2\pi/k$ to the mean free path between collisions,

$$y = \frac{p}{kv_0\eta} = \frac{nk_BT}{kv_0\eta}, \tag{1}$$

where $k = |\boldsymbol{k}_s - \boldsymbol{k}_p|$ is the scattering wave vector, n is the number density, T is the temperature, p is the pressure, v_0 is the thermal velocity, $v_0 = (2k_BT/M)^{1/2}$, η is the (shear) viscosity, and k_B is the Boltzmann constant. The definition of y is based on the simple (dimensional) relationship between the mean free path between collisions and the shear viscosity η. The parameter y can be viewed as the dimensionless pressure or the dimensionless wavelength.

In the kinetic regime $0.3 \lesssim y \lesssim 3$, which is the relevant regime for this article, neither the individual-particle approach nor the continuum approach applies, and one has to resort to solving the Boltzmann equation for the density fluctuations. At even smaller y, the density is so low that we enter the Knudsen regime and the scattering is solely due to individual thermal molecules. In this case, the wavelength dependence of scattered radiation is given by the Rayleigh distribution,

$$I(k,\omega) = \frac{2\pi^{1/2}}{kv_0}e^{-x^2}, \tag{2}$$

with the dimensionless frequency $x = \omega/(kv_0)$. In principle, the solution of the Boltzmann equation is determined by the cross section of elastic and inelastic collisions between molecules and, in principle, detailed knowledge about the collision cross sections would be needed. However, such knowledge is not available and therefore collision models must be devised.

The starting point of line-shape models is the linearized Boltzmann equation, which describes the deviation $h(\boldsymbol{r},\boldsymbol{v},t)$ of the position-velocity distribution function from its form at thermal equilibrium, the Maxwellian $\phi(v)$. The hydrodynamic variables, such as density, velocity, and heat flux are the velocity moments of $f(\boldsymbol{r},\boldsymbol{v},t) = \phi(v)[1 + h(\boldsymbol{r},\boldsymbol{v},t)]$. The linearized collision operator is approximated using the method of Wang Chang and Uhlenbeck, which constructs the collision integral from the transport coefficients [31].

In the now well-known Tenti S6 and S7 models, the perturbation h of the position-velocity probability density function is expanded in eigenfunctions of the linearized collision operator for molecules that interact with intermolecular force $F \sim r^{-5}$ [4,5] and is truncated after 6 or 7 terms. It was shown in [5] that, from the two truncations, surprisingly the 6-moment model (the Tenti S6 model) provides the superior fit of experimentally measured line shapes, probably because of an effective resummation of the truncated expansion.

These line-shape models recycle information: from known values of the transport coefficients of the continuum regime that is the macroscopic flow of gases, they reconstruct the collision operator needed in the kinetic approach. Two errors can arise in this procedure: (i) the truncation of the collision operator is not adequate, and (ii) the transport coefficients are not known precisely.

For a single-species gas, the transport coefficients needed are the shear viscosity η, the thermal conductivity λ, the heat capacity c_{int} of the internal degrees of freedom, and the bulk viscosity η_{b}. Of these transport coefficients, the bulk viscosity is essentially dependent on the frequency. Its known value has been determined mostly in experiments involving ultrasound but, because frequencies in light scattering are much larger, η_{b} must be considered as poorly known in this range.

In the spontaneous case, Rayleigh-Brillouin scattering is due to the decay of density waves with wave numbers set by the scattering wave number k. An interesting twist to the problem of Rayleigh-Brillouin scattering was given quite recently by experiments and theory on coherent Rayleigh-Brillouin scattering [24]. It differs from spontaneous Rayleigh-Brillouin scattering in that density fluctuations are now induced by subjecting the molecules to dipole forces in the electric field of a standing light wave. In this case, the linearized Boltzmann equation needs to be augmented by the velocity-changing dipole-force term $\boldsymbol{a} \cdot \boldsymbol{\nabla}_v \phi$, with $\boldsymbol{a}$ being the dipole force, that directly acts on the zero-order Maxwellian $\phi(v)$,[1]

$$\left(\frac{\partial}{\partial t} + \boldsymbol{v} \cdot \boldsymbol{\nabla} \right) h + \boldsymbol{a} \cdot \boldsymbol{\nabla}_v \phi = J[h], \qquad (3)$$

where $J[h]$ is the linearized collision operator acting on the perturbation h. Otherwise, the treatment of the collision operator J proceeds in precisely the same manner as for spontaneous Rayleigh-Brillouin scattering. This was described in a nice didactical article by Pan *et al.* [24]. In coherent Rayleigh-Brillouin scattering, light is scattered by the induced dipoles, such that the scattered radiation inherits coherence from the optical wave field and is concentrated in a beam that

points in the direction determined by 4-wave phase-matching conditions. This results in a tremendous increase in the signal, and a complete Rayleigh-Brillouin spectrum can be registered in a single laser shot. However, the spectral width of the pump field must be larger than the spectral width of the Rayleigh-scattered radiation, and creating a smooth broad-band line shape is a challenge when using pulsed lasers.

The kinetic models for the line shape of coherent Rayleigh-Brillouin scattering need exactly the same macroscopic information as those for spontaneous Rayleigh-Brillouin scattering and are described by the same approximated collision integral. However, the spectra are different and thus provide a different magnifying glass on the accuracy of these models. The dipole force $\boldsymbol{a}$ is determined by the pump-beam intensity and by the polarizability α of the molecules. For a single-species gas, information about α is not needed, as it is a mere scale factor of the spectra. Information about α for the dipole forces is only needed for a mixture of gases. However, in this case the same information would be needed for spontaneous Rayleigh-Brillouin scattering, because the scattering intensity is also proportional to α.

For spontaneous Rayleigh-Brillouin scattering, the spectral line shape $I(k,\omega)$ is proportional to the real part of the first moment $v(k,\omega)$ of $f(\boldsymbol{r},\boldsymbol{v},t)$ in Fourier space, whereas for coherent scattering it is proportional to $|v(k,\omega)|^2$. This distinction rests in a subtle difference in interpretation of the Boltzmann equation, which for spontaneous Rayleigh-Brillouin scattering describes an initial value problem.

Although the Tenti models have considerable algebraic complexity, their evaluation only involves the diagonalization of a small matrix and the evaluation of the error function, which can be done extremely quickly on a computer.

III. MIXTURES OF GASES

The Tenti S6 and S7 line-shape models are for gases consisting of a single kind of molecule. However, natural air, the object of many applications of light scattering, is a mixture of several gases. Each of those components has its own molecular structure and its own collision cross section. Moreover, if the components of a mixture have different mass or different collision cross sections, another relaxation mechanism arises when equilibration of translational energy between the species requires several collision times τ_{c}.

A naive but perhaps effective approach may be to consider air as a fictitious gas, with effective transport coefficients determined by molecules with an effective mass and effective internal degrees of freedom. While such an approach may work, it is not internally consistent because the effective kinetic parameters are not well defined, and an agreement between model and experiment must be deemed fortuitous. Still, in a separate study on spontaneous Rayleigh-Brillouin scattering on dry and moist air, measured spectra could be well-represented by the Tenti S6 model, taking the effective transport coefficients of air as parameters [32].

Brillouin light scattering experiments on mixtures have been done by the group of Letamendia *et al.* [18,19]. Their key point was that, in mixtures of noble gases with a very large disparity of masses (for example Xe and He), thermal equilibrium is reached slowly due to the inefficiency

---

[1]Implicit is an ordering of small parameters where the dipole term is of the same order as the perturbation $\phi(v)\,h(\boldsymbol{r},\boldsymbol{v},t)$.

of the energy transfer by collisions, and the constituents have effectively two temperatures. A kinetic model for both coherent and spontaneous Rayleigh-Brillouin scattering has been published by Marquez [7,8] and provides an improved reproduction of the spectra (over the hydrodynamical model that was originally tried by Letamendia [18,19]).

The macroscopic description of mixtures requires many more transport coefficients whose values are not always known precisely. The solution followed in [7,8] is to view the molecules as hard spheres. For hard spheres, all transport coefficients, including the mixture ones, follow from the hard-sphere radius, which can be computed from the shear viscosity. The disadvantage of such a treatment is that no effects of the internal degrees of freedom can be described in this manner.

As this model should work well for a simple noble gas, we shall compare it to scattering experiments on Kr. We also compare this model to experiments involving mixtures of both atomic and molecular gases. We argue that new models must be designed that allow for mixtures of molecules with internal degrees of freedom.

IV. THE BULK VISCOSITY

The macroscopic continuum description of gases, as is embodied by the Navier-Stokes equation, is based on a simple linear relationship between cause and effect, that is, strain and stress. In an isotropic medium, this relation leaves two proportionality constants, the shear viscosity and the bulk viscosity. Normally, only the shear viscosity is retained (the Stokes assumption), but whether this is justified or not can only be decided based on microscopic information about the structure of the gas molecules [33]. The origin of the bulk viscosity is the relaxation of the internal degrees of freedom of a molecule in collisions. Usually, the associated relaxation time τ_i is a multiple of the mean time between collisions. So far, all experimental information about η_b comes from measurements of the absorption of ultrasonic waves, which are difficult measurements to interpret [34]. Due to the emergence of the time constant τ_i, the bulk viscosity depends on the frequency of sound. As in light scattering experiments, the probed wave numbers and, consequently, the sound frequencies, are at least 1 to 2 orders of magnitude larger than in acoustical experiments, so the currently known values of η_b may not be reliable for light scattering. Therefore, we will try systematically to obtain a better reproduction of measured line profiles by varying η_b.

There is a delicate interplay between molecular structure and the frequency of sound. If vibrational levels have energies comparable to $k_B T$ and therefore can be reached in collisions, they generally come with very long relaxation times τ_i, and thus large values of η_b. However, these excited vibrational levels may remain frozen in light scattering experiments because of the high frequencies involved. A survey of the bulk viscosity of many other polar and nonpolar molecules using coherent Rayleigh-Brillouin scattering has recently been done in [35].

While the bulk viscosity η_b may provide a convenient parameter in which internal molecular degrees of freedom can be lumped, its fundamental basis remains highly controversial [36]. Perhaps, the only correct manner to describe gases with internal degrees of freedom would be to treat each internal state as separate species in a multicomponent kinetic theory.

V. EXPERIMENTAL SETUPS

In a joint effort to study Rayleigh-Brillouin scattering in both the spontaneous and coherent arrangement, we built two different experimental setups which we will now briefly describe. Further details can be found in [32,35].

The spontaneous scattering experiment was inspired by the future ESA Earth Explorer Atmospheric Dynamics Mission, which will provide global observations of wind profiles from space [6]. In this satellite mission, an ultraviolet laser beam (at 355 nm) will be backscattered off the atmosphere. Our spontaneous scattering experiments also use ultraviolet light, but practical considerations dictated a 90° scattering angle and a wavelength of 366.5 nm. These conditions result in a scattering wave vector $k = 2.43 \times 10^7$ m^{-1}. The coherent experiment operates with visible light (532 nm), but with a nearly 180° scattering angle. Consequently, the wave vector $k = 2.36 \times 10^7$ m^{-1} has a comparable size to the wave vector of the spontaneous case.

A. Coherent Rayleigh-Brillouin scattering

The experimental setup follows the two-dimensional backward scattering configuration of Pan *et al.* [37]. A diagram of the setup is shown in Fig. 1. Two broad-band pump laser beams with wave vectors k_1 and k_2 are focused with 500-mm focal-length lenses and cross at their foci under an angle of 178°. The counterpropagating beams form multiple optical gratings in which gas molecules are polarized and subjected to a force toward the high-electric-field regions. This dipole force creates moving periodic density perturbations in the gas with angular frequency $\omega = \omega_1 - \omega_2$ and propagation vector $k = k_1 - k_2$
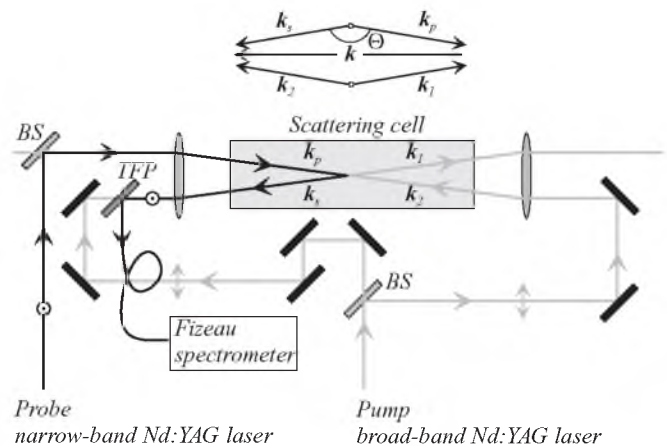

FIG. 1. Schematic of the experimental setup for coherent Rayleigh-Brillouin scattering (not to scale). The counterpropagating pump beams with wave vectors k_1, k_2 are indicated in grey; the probe laser beam with wave vector k_p and the scattered light beam with k_s are black. The scattered light is collected in a single-mode optical fiber and transported to the Fizeau spectrometer. A thin-film polarizer is indicated by TFP, beam splitters by BS. The polarization directions are indicated by ↕ and ⊙. The arrangement of the wave vectors corresponding to the phase-matching condition is indicated.

perpendicular to the fringes. Due to the wide bandwidth of the pump laser, the generated density perturbations also have a wide spectral distribution. The density waves are probed by Bragg diffraction off the induced density gratings of a narrow-band laser with wave vector $\boldsymbol{k}_p$. Optical coherence requires phase matching with, in our experiment, the consequence that the signal beam $\boldsymbol{k}_s$ propagates in the opposite direction to the pump beam $\boldsymbol{k}_1$, $\boldsymbol{k}_2 - \boldsymbol{k}_1 = \boldsymbol{k} = \boldsymbol{k}_s - \boldsymbol{k}_p$. The signal beam maintains the probe beam's characteristics, such as its polarization, but it will be spectrally broadened due to the interaction with the broad superposition of sound waves with frequency $\omega_s - \omega_p = \omega = \omega_1 - \omega_2$.

The gas to be investigated is inside a stainless steel cell of 0.5-m length equipped with optical windows. The cell allows for control of the gas conditions such as composition and pressure. The pump laser is a Q-switched frequency-doubled broad-band Nd:YAG laser with 10-ns pulse duration (manufactured by Quantel). The laser bandwidth is estimated to be 24 GHz full width half maximum (FWHM) with a 250-MHz mode structure. The narrow-band probe laser is an injection-seeded frequency-doubled pulsed Nd:YAG laser with a FWHM of 150 MHz and 7-ns pulse duration (manufactured by Spectra Physics). Typical pulse energies are 8 mJ and 2 mJ for the pump and probe beams, respectively. As the peak power densities remain much smaller than 10^{15} Wm^{-2}, our experiment is in the perturbative regime [38,39].

The probe beam is polarized perpendicularly with respect to the polarization of the pump beams, and the signal beam is separated from the pump beam path using a thin film polarizer. This arrangement avoids possible interferences between pump and probe beams and its associated complexities.

A customized fiber-coupled Fizeau spectrometer (Angstrom Co Ltd, HighFinesse GmbH) is used to measure the scattered-frequency distribution. The Fizeau spectrometer is based on the same fundamental principles of multiple beam interference as a Fabry-Perot etalon [40]. The advantage of this device is that all frequencies are measured simultaneously. The spectrum is directly imaged onto a charge-coupled device (CCD) array, with a simple relationship between frequency and position. As the mirrors in the Fizeau spectrometer are not parallel, the spectral response to monochromatic light is slightly asymmetric [41–43]. This was measured in a separate experiment, and the result was used to convolve the Rayleigh-Brillouin scattering spectra computed from the Tenti model. The distance between the mirrors determines the FSR, the mirror reflectivity determines the finesse, and the wedge angle determines the spectral dispersion. The Fizeau spectrometer has an FSR of 10.06 GHz, a finesse of 56, and a resolution of 250 MHz.

The presence of the longitudinal mode structure of the pump laser, which randomly fluctuates between successive pulses, is the largest source of noise in the registered coherent Rayleigh-Brillouin spectra and necessitates averaging of the spectrum over multiple laser shots. Our spectra are the average over 10 independent spectra, each of which is an average over 500 laser shots. Consequently, each spectrum is acquired in approximately 8 minutes. Long-time averages would show the periodic mode structure of the pump laser multiplied with the spectrum. However, since the resolution of the spectrometer equals the mode spacing of the pump laser, the mode structure
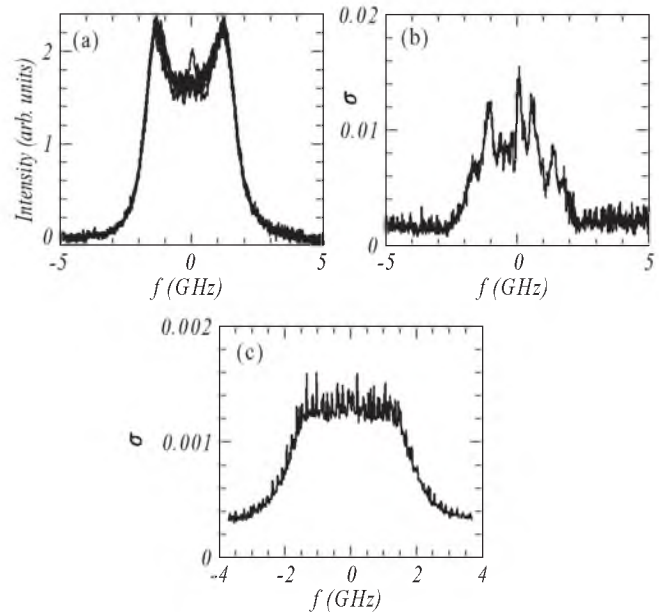

FIG. 2. The fluctuations of measured Rayleigh-Brillouin scattering spectra in N_2 at $p = 3$ bar. (a), (b) Coherent scattering experiments: (a) Superposition of spectra, each averaged over 500 laser shots, (b) Root-mean-square fluctuation $\sigma(f)$ of registered spectra estimated from the spectra in (a). The scale is the same as that of the mean spectrum in Fig. 7(b). (c) Photon noise $\sigma(f)$ for the spontaneous Rayleigh-Brillouin scattering spectrum N_2 at $p = 3$ bar.

is barely visible in the Rayleigh-Brillouin spectra, and it was not necessary to remove it by filtering, as was done in [37].

The statistical error in the found η_b is determined by the statistical fluctuations in the measured spectra. From the variation in the 10 registered spectra, we estimate the rms variation at each (discrete) frequency $\sigma(f_i)$, as is illustrated in Figs. 2(a) and 2(b).

In principle, accurate single-shot coherent Rayleigh-Brillouin spectra are possible using a pump laser with a smooth and reproducible broad-band spectrum. In this way, the instantaneous density and temperature of a gas would
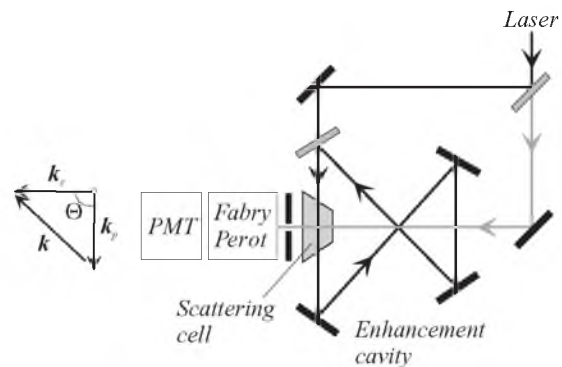

FIG. 3. Schematic of the experimental setup for spontaneous Rayleigh-Brillouin scattering (not to scale). The UV laser beam (full black line) is reflected several times in the enhancement cavity to increase the scattering intensity. A reference beam (gray line), split off from the main beam, is used for detector alignment. Scattered light is detected at 90° using a pinhole, a Fabry-Perot interferometer, and a photomultiplier (PMT).

be accessible using coherent Rayleigh-Brillouin scattering. Clearly, this goal has not yet been achieved.

B. Spontaneous Rayleigh-Brillouin scattering

A schematic view of the setup for spontaneous Rayleigh-Brillouin scattering is shown in Fig. 3. The light from a narrowband continuous wave laser is scattered off a gas contained in a temperature-controlled gas cell. The laser is a frequency doubled Ti:Sa laser delivering light at 366.5 nm, 2-MHz bandwidth, and with 400 mW of output power. The long-term frequency drift was measured with a wavelength meter to be smaller than 10 MHz per hour. The scattered light is collected at an angle of $90°$ from an auxiliary focus inside the enhancement cavity, in which a scattering cell is mounted. The cell is sealed with Brewster windows. The circulation of the light inside the enhancement cavity amplifies the power by a factor of 10.

The scattering angle is calculated to be $90° \pm 0.9°$ by means of the reference laser beam and geometrical relationships using sets of diaphragms and pinholes present in the optical setup. The scattered light is filtered by a diaphragm which covers an opening angle of $2°$, collected by a set of lenses, further filtered by an extra pinhole ($d = 50$ μm), and then directed into a hemispherical scanning Fabry-Perot interferometer (FPI), which is used to resolve the frequency spectrum of the scattered light. To scan the FPI-plate distance, the spherical mirror is mounted on a piezoelectric translator, which is controlled by a computer.

The spectral response $S(f)$ of the Fabry-Perot spectrometer was measured in a separate experiment, and could be parametrized very well by the formula

$$S(f) = \left[1 + \left(\frac{2f_{FSR}}{\pi f_{w}} \sin \frac{\pi f}{f_{FSR}} \right)^2 \right]^{-1}, \quad (4)$$

where f_{FSR} is the free spectral range of the etalon ($f_{FSR} =$ 7440 MHz), and $f_{w} = 232$ MHz is the Airy width of the transmission peak. All computed model spectra were
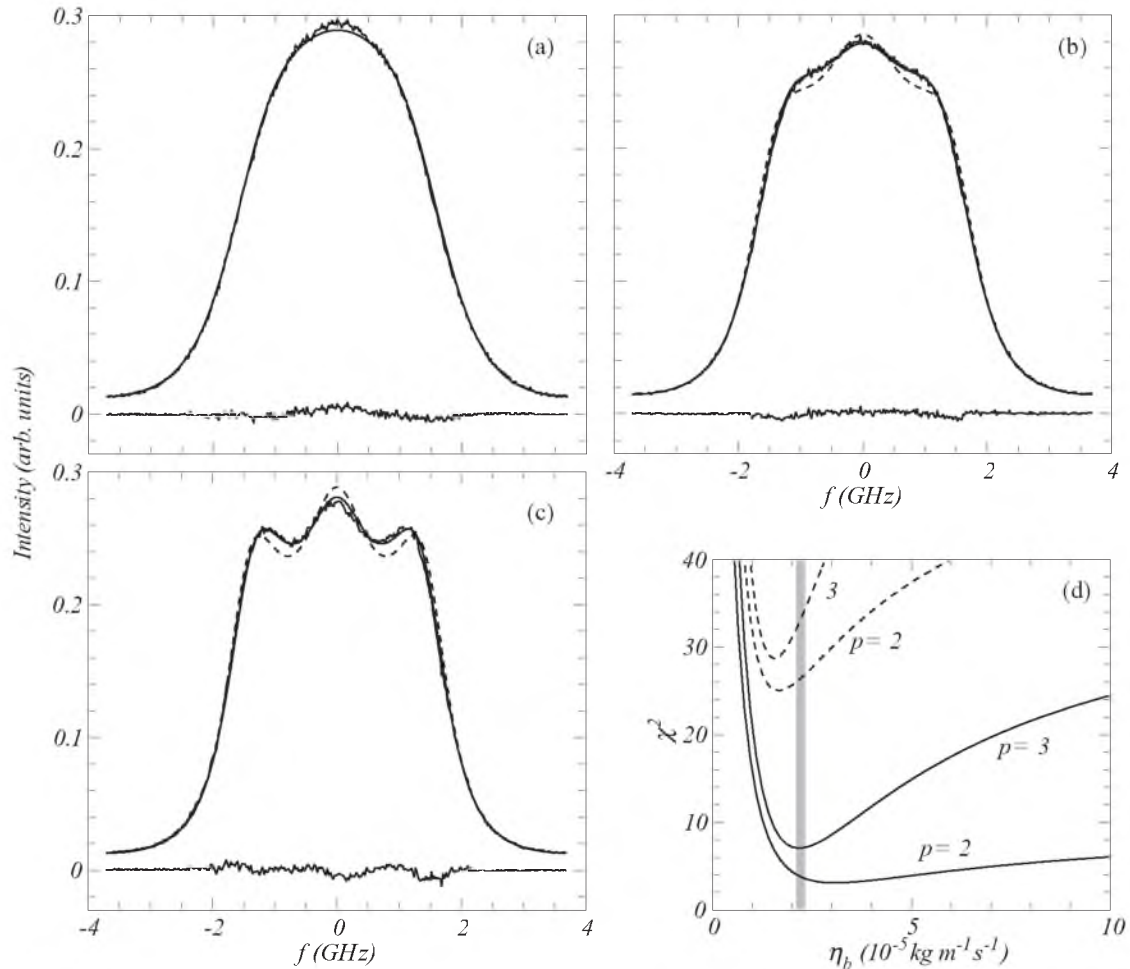

FIG. 4. N_2 spontaneous Rayleigh-Brillouin scattering for increasing pressures, $p = 1$, 2, and 3 bar for (a), (b), and (c), respectively. The dimensionless pressures are $y = 0.60$, 1.15, and 1.67, respectively. Full lines correspond to model spectra computed using the Tenti S6 model, dashed lines correspond to model spectra using the Tenti S7 model. Lower full line indicates the difference between experiment and Tenti S6 model. (d) χ^2 error as a function of bulk viscosity η_b; full lines correspond to model spectra using the S6 model, dashed lines correspond to model spectra using the S7 model. The overall higher values of χ^2 show that the spectra are not well described by the S7 model. The χ^2 error at $p = 3$ using the S6 model has a minimum at $\eta_b = 2.2 \times 10^{-5}$ kg m^{-1} s^{-1}, which is indicated by the grey line; the value of η_b at smaller pressures cannot be determined in this way.

convolved with $S(f)$ and, since the free spectral range is relatively small, it is important to allow for the periodic nature of $S(f)$.

The light that passes through the FPI is detected using a photomultiplier tube (PMT), which is operated in the photon-counting mode and read out by a computer. To prevent contamination on the mirrors that could lead to absorption of UV light, the enhancement cavity as well as the FPI is flushed with dry nitrogen. Inside the cell, the pressure is measured with an active piezo transmitter (Pfeiffer-APR). The temperature is measured with a thermo resistor Pt100. Before performing a measurement, the scattering cell was evacuated and purged with the working gas, before being charged to the desired pressure, to a avoid any contamination from gases of previous measurements. The temperature for all measurements ranged between 295 and 303 K.

Assuming Poissonian statistics of registered photon counts, an estimate of the statistical error $\sigma(f)$ of measured spectra

was obtained from the square root of the accumulated photon count N_i at each discrete frequency f_i. It was verified that the fluctuations $N_i^{1/2}$ at each f_i were independent. The statistical error is shown in Fig. 2(c); it is approximately one order of magnitude smaller than that of the coherent experiments.

VI. NORMALIZATION OF MEASURED SPECTRA

The light-scattering experiments do not provide an absolute intensity, therefore the experimental and computed spectra were normalized such that $\int_{-f_b}^{f_b} I(f) df = 1$, where the integral extends over one FSR ($f_b = f_{FSR}/2$). Ideally, the bounds f_b of the integration should be such that $I(\pm f_b) = 0$; however, for the spontaneous Rayleigh-Brillouin scattering experiments, the FSR of the etalon is not much larger than the width of the measured spectra, which for air molecules is approximately 4×10^9 Hz, and it is important to realize how the spectra are normalized. Since the FSR of the
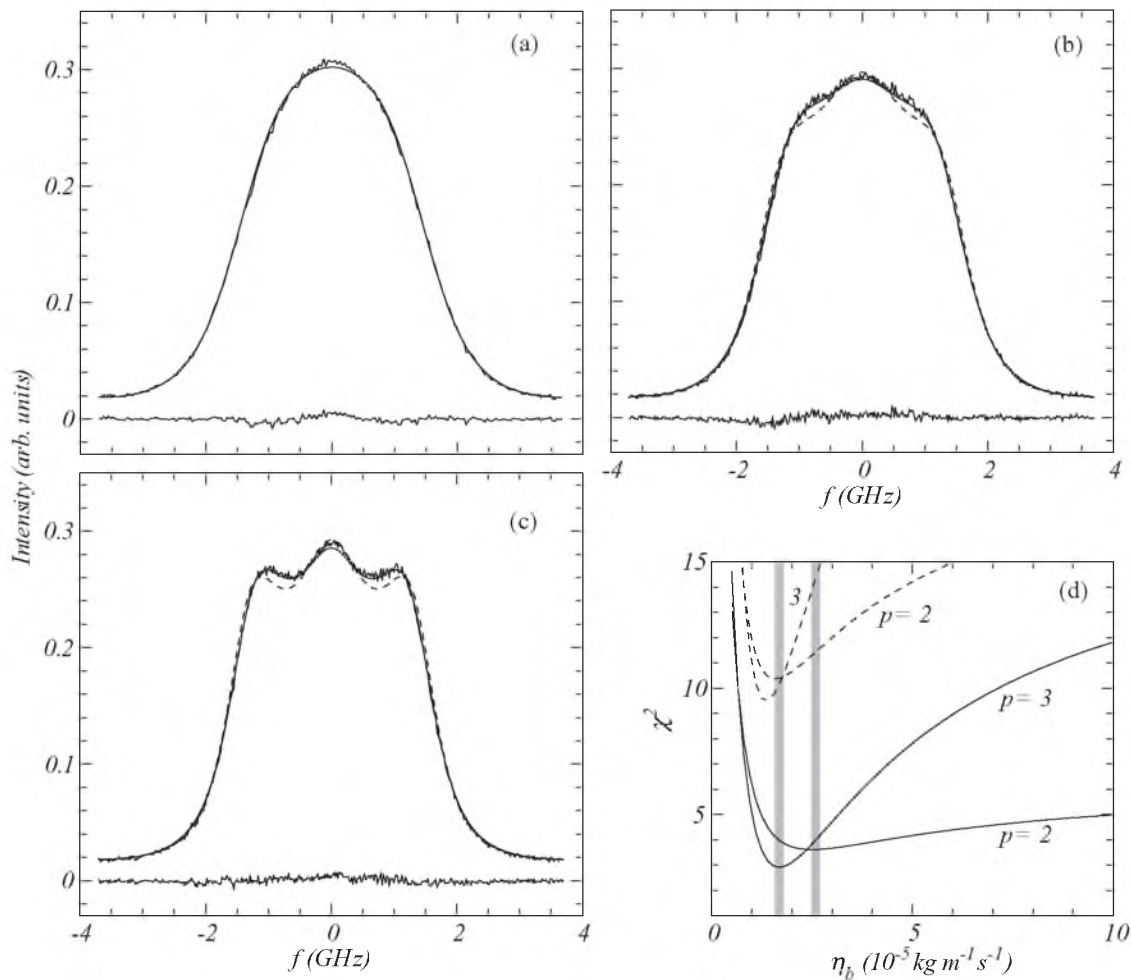

FIG. 5. O_2 spontaneous Rayleigh-Brillouin scattering for increasing pressures, $p = 1$, 2, and 3 bar for (a), (b), and (c), respectively. The dimensionless pressures are $y = 0.51$, 1.05, and 1.54, respectively. Full lines correspond to model spectra computed using the Tenti S6 model, dashed lines correspond to model spectra using the Tenti S7 model. For $p = 1$ and 2 bar, the model spectra were computed using $\eta_b = 2.6 \times 10^{-5}$ kg m^{-1} s^{-1}, while for 3 bar, $\eta_b = 1.75 \times 10^{-5}$ kg m^{-1} s^{-1}. Lower full line shows the difference between experiment and the Tenti S6 model. (d) χ^2 error as a function of η_b; full lines are using the S6 model, dashed lines are using the S7 model. The overall higher values of χ^2 show that the spectra are not well described by the S7 model. Using the S6 model, the error at $p = 2$ has a minimum at $\eta_b = 2.6 \times 10^{-5}$ kg m^{-1} s^{-1}, while at $p = 3$, the minimum is at $\eta_b = 1.75 \times 10^{-5}$ kg m^{-1} s^{-1}. These two minima are indicated by the gray lines.

Fizeau spectrometer used in the coherent Rayleigh-Brillouin scattering experiment is always (much) larger than the width of our Doppler-broadened lines, the precise value of f_b is not important for the coherent case.

Another issue is the signal background I_{e_0} in the experiment, which must be subtracted from the raw measured spectrum $I_{e_r}(f)$ before normalization of $I_e(f) = I_{e_r}(f) - I_{e_0}$. In the spontaneous Rayleigh-Brillouin experiments, I_{e_0} is mainly made up of dark counts of the photomultiplier; it was determined for each measurement and was subtracted from the subsequently measured spectrum. However, it turns out that I_{e_0} also contains a small contribution I'_{e_0} of broadband fluorescence of the cell windows. We discovered that this contribution also depends on the exposure history of the cell windows.

Therefore, it was decided to correct the model spectra $I_m(f)$ for this residual background contribution by setting $I_m(f) = aI_e(f) - I'_{e_0}$, and to determine I'_{e_0} and the proportionality constant a in a least-squares procedure for the wings of the spectra, where the wings are defined as frequencies such that $I_m(f) \leqslant \max(I_m)/4$. The idea is that it is better to use the wings of a model spectrum rather than fitting a horizontal line to the background. If the measured spectra would have the correct background, $a = 1$ and $I'_{e_0} = 0$. The shifted model spectrum $I'_m(f) = I_m(f) + I'_{e_0}$ was then normalized again such that $\int_{-f_b}^{f_b} I'_m(f)df = 1$. This procedure, which converges quickly, gives a small but perceptible shift of the background.

In the coherent Rayleigh-Brillouin scattering experiments, the background is mainly made up of dark current of the (uncooled) CCD array in the Fizeau spectrometer. It is large, and of the order of the signal strength. It was determined following the same procedure as explained above involving the wings of the spectra, with I_{e_0} determined in a least-squares procedure through $I_m(f) = a[I_e(f) - I_{e_0}]$. Finally, as the origin of the frequency scale of the Fizeau spectrometer is not well determined, both measured and model spectra were shifted so that their centers lie at $f = 0$.

To summarize, normalization of the measured spectra also involves the determination of the background from a comparison with the computed model spectrum. For the spontaneous Rayleigh-Brillouin scattering experiments, this is a small correction added to the experimentally determined background. For the coherent Rayleigh-Brillouin scattering experiment, it is an essential part of the normalization procedure.

Let us now quantify the difference between the experiment and the computed model spectra. Using the estimated error $\sigma(f_i)$ in the measured spectra at discrete frequencies f_i ($i = 1, \ldots, N$), we compute the normalized difference $\Delta(f_i)$ between model $I_m(f_i)$ and experimental $I_e(f_i)$ spectra as $\Delta(f_i) = [I_m(f_i) - I_e(f_i)]/\sigma(f_i)$, and the normalized error as $\chi^2 = N^{-1} \sum_{i=1}^{N} \Delta^2(f_i)$. If the computed line-shape model I_m fits the measurement perfectly, then only statistical errors remain and the minimum of χ^2 is unity. Let $\tilde{\eta}_b$ be the value of η_b at which χ^2 has a minimum. Using a maximum likelihood argument, the curvature of the function $\chi^2(\eta_b)$ in this point determines the error in the estimation of the bulk viscosity via

$$\sigma_{\eta_b} = \left(\frac{N'}{2} \frac{d^2\chi^2}{d\eta_b^2} \bigg|_{\tilde{\eta}_b} \right)^{-1/2}, \tag{5}$$
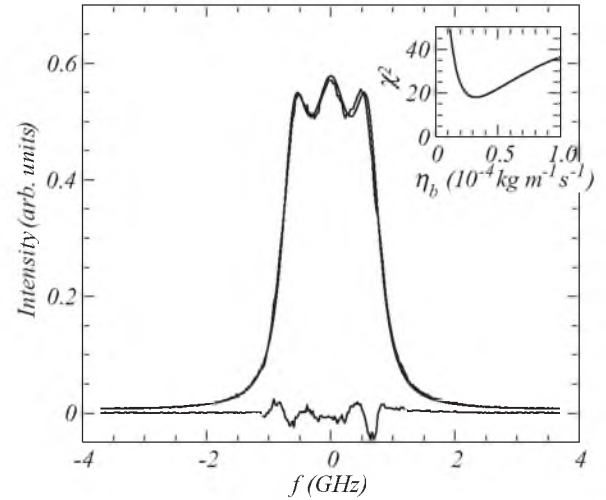

FIG. 6. SF_6 spontaneous Rayleigh-Brillouin scattering at $p = 1.95$ bar compared to the Tenti S6 model, which was computed taking $\eta_b = 3.5 \times 10^{-5}$ kg m^{-1} s^{-1}. Lower full line shows the difference between experiment and the Tenti S6 model. Inset shows the χ^2 error as a function of η_b. In this experiment, the sound frequency is $f = 575$ MHz, which follows from $c_{int} = 3/2$ and the scattering wave vector $k = 2.42 \times 10^7$ m^{-1}.

where N' is the number of independent samples in the spectrum. For the coherent experiment, N' is determined by the mode fluctuations of the pump laser, with the spectral width of a mode spanning several discrete frequency intervals. For the spontaneous experiments in which the frequency is scanned in time and the shot-noise fluctuations at each discrete pixel are independent, N' equals the number of discrete frequency samples. We should realize, however, that σ_{η_b} is merely the statistical error in the measured η_b. An important source of systematic error is the alignment of the setup.

VII. RESULTS

The purpose of the experiments is to obtain precise spectra of simple gases, both for the spontaneous and the coherent

TABLE I. Values of the transport coefficients used in the computation of line-shape models: the shear viscosity η, the heat conductivity λ, and the dimensionless heat capacity c_{int} of internal degrees of freedom. For the line-shape model for mixtures, the hard-sphere radius σ and the polarizability α is listed. The transport coefficients are given at a reference temperature $T = 293$ K, but the actual values used were corrected for the temperature of each experiment.

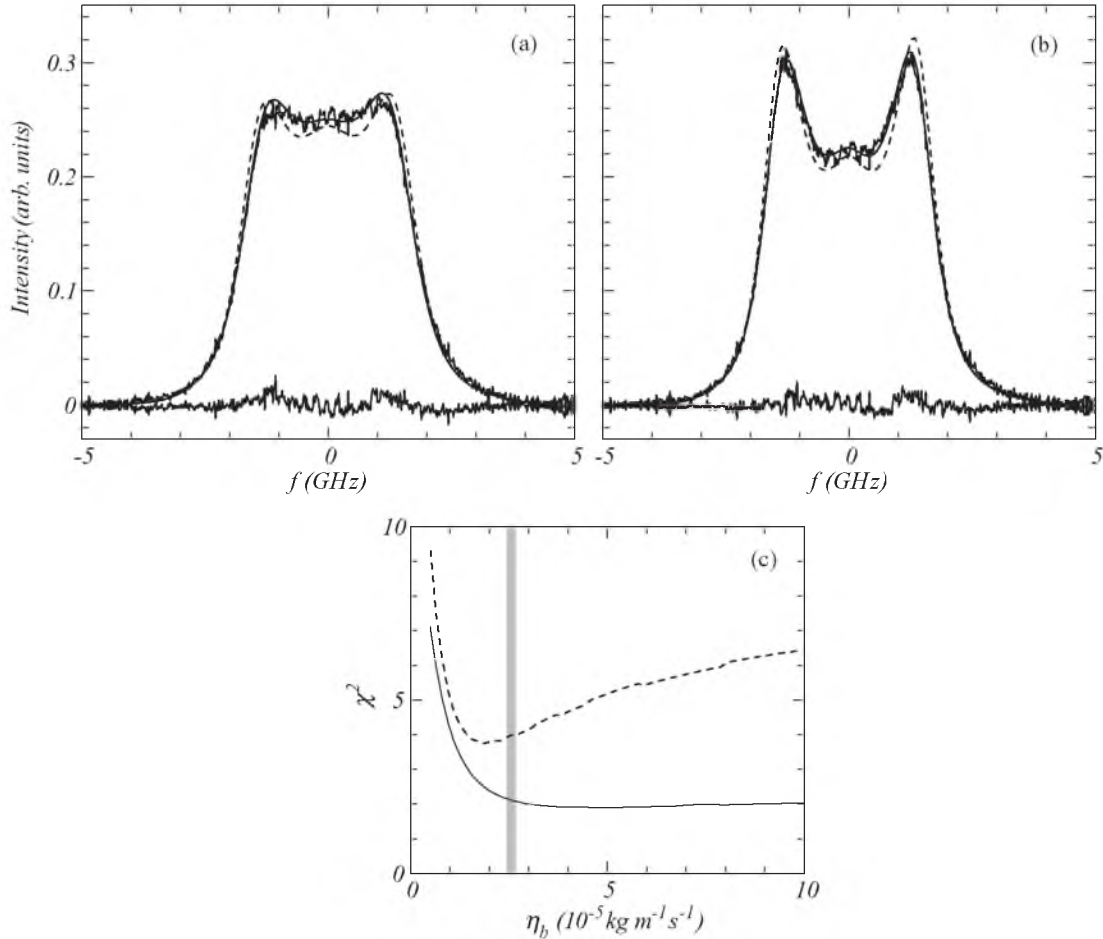|	η (10^{-5} kg m^{-1} s^{-1})	λ (10^{-2} W K^{-1} m^{-1})	c_{int}	σ (10^{-10} m)	α (10^{-40} C m^2 V^{-1})
N_2	1.77	2.52	1		
O_2	2.02	2.02	1		
CO_2	1.46	1.62	1		
SF_6	1.49	1.31	3/2		
He	1.97	15.4	0	2.16	0.227
Kr	2.50	0.93	0	4.20	2.94
Xe	2.28	0.54	0	4.90	4.46

FIG. 7. N_2 coherent Rayleigh-Brillouin scattering for $p = 2$ and 3 bar in (a) and (b), respectively. The dimensionless pressures are $y = 1.15$ and 1.73, respectively. Full lines show the model spectra computed using the Tenti S6 model and dashed lines show the model spectra using the Tenti S7 model. The model spectra were computed for $\eta_b = 2.6 \times 10^{-5}$ kg m^{-1} s^{-1}. Lower full line shows the difference between experiment and the Tenti S6 model. The spectra are slightly asymmetric due to the asymmetry of the Fizeau spectral response (Sec. V A). (c) χ^2 error as a function of η_b for $p = 3$ bar; the full line is using the S6 model, the dashed line is using the S7 model. The grey line indicates the minimum of χ^2 found at $p = 5$ bar [35].

arrangement and to establish the accuracy of line-shape models. At the same time, a value of the bulk viscosity is obtained using the least-squares procedure explained in Sec. VI. Finally, coherent Rayleigh-Brillouin spectra of gas mixtures will be compared to a recent line-shape model.

A list of the transport coefficients used for computation of the line-shape models is given in Table I. The transport coefficients are given at a reference temperature $T = 293$ K, but the actual values used were corrected for the temperature of each experiment using a $T^{1/2}$ dependence of η and λ, which is adequate for small temperature differences.

A. Spontaneous Rayleigh-Brillouin scattering

Spontaneous Rayleigh-Brillouin line shapes for N_2 are shown in Fig. 4 for a range of pressures. All spectra are very well described by the Tenti S6 model, whereas the 7-moment model differs significantly from the experimental data. Of course, this was already known to Tenti *et al.* [5] for a

gas of HD molecules.[2] The slight discrepancy at the lowest pressure (where the scattered light intensity is weakest) may be due to reflected light. At $p = 3$ bar, the measured χ^2 has a clear minimum at $\eta_b = 2.2 \times 10^{-5}$ kg m^{-1} s^{-1}. Using the properties of this minimum, and following Eq. (5), we estimate a statistical error of approximately 1%. We believe that this error is not representative of the uncertainty in η_b, which is mainly determined by systematic errors.

The value $\eta_b = 2.2 \times 10^{-5}$ kg m^{-1} s^{-1} that we find is much larger than $\eta_b = 1.28 \times 10^{-5}$ kg m^{-1} s^{-1} found in the literature; a value which was determined at acoustical frequencies [44], but verified by Lao *et al.* in light scattering experiments [13].

Spontaneous Rayleigh-Brillouin line shapes for O_2 are shown in Fig. 5 for a range of pressures. As for N_2, all spectra

---

[2]For the computation of the S7 model, we have used the same program as in [24], which for HD gives a different result than that shown by Tenti *et al.* [5]. In [5], the difference between the S6 and S7 model is much larger than in [24] and the present article. Possibly, [5] made an error in the implementation of their S7 model.

are very well described by the Tenti S6 model, whereas the 7-moment model differs significantly from the experimental data. At $p = 3$ bar, the measured χ^2 has a clear minimum at $\eta_b = 1.75 \times 10^{-5}$ kg m^{-1} s^{-1}, whereas at $p = 2$ bar the minimum is at $\eta_b = 2.6 \times 10^{-5}$ kg m^{-1} s^{-1}. Because no minimum can be observed for lower pressures, the spectrum at $p = 1$ bar was computed using $\eta_b = 2.6 \times 10^{-5}$ kg m^{-1} s^{-1}. The values of η_b that we find for O$_2$ are much larger than the value $\eta_b = 0.82 \times 10^{-5}$ kg m^{-1} s^{-1} found in the literature, which was determined in acoustical experiments [45].

Since complex molecules have many internal degrees of freedom, which may or may not relax quickly enough in light scattering experiments, it is interesting to revisit their bulk viscosity. Figure 6 shows a spontaneous Rayleigh-Brillouin spectrum in SF$_6$ at $p = 2$ bar, together with the dependence of χ^2 on η_b.

Spontaneous Rayleigh-Brillouin scattering of SF$_6$ has been studied by Clark *et al.* at a scattering angle of $11°$ and a wavelength of 633 nm; consequently, the sound frequency was more than one order of magnitude smaller than in the present experiment [46]. The vibrational levels of SF$_6$ have a long

relaxation time ($\approx 2 \times 10^{-7}$ s) and therefore remain frozen in light scattering experiments. The rotational relaxation time is also relatively slow ($\approx 6 \times 10^{-10}$ s). While Clark *et al.* concluded that rotational levels partake in relaxation and thus contribute a bulk viscosity, this may be different in our experiments. Nevertheless, in the analysis of our experiment we take $c_{int} = 3/2$ for the heat capacity of internal degrees of freedom.

Figure 6 shows a minimum of the χ^2 error at $\eta_b = 3.5 \times 10^{-5}$ kg m^{-1} s^{-1}, which can be compared to the value documented in the literature ($\eta_b = 2.03 \times 10^{-5}$ kg m^{-1} s^{-1}) [47]. This result is puzzling as we would have expected a smaller η_b at our sound frequency ($f \approx 600$ MHz). Clearly, the limited frequency resolution of our experiment (232 MHz) does not allow further conclusions.

B. Coherent Rayleigh-Brillouin scattering

In Fig. 7, we show coherent Rayleigh-Brillouin spectra of N$_2$ at pressures $p = 2$ and 3 bar. Due to the fluctuating mode structure of the pump laser, the noise in the measured spectrum
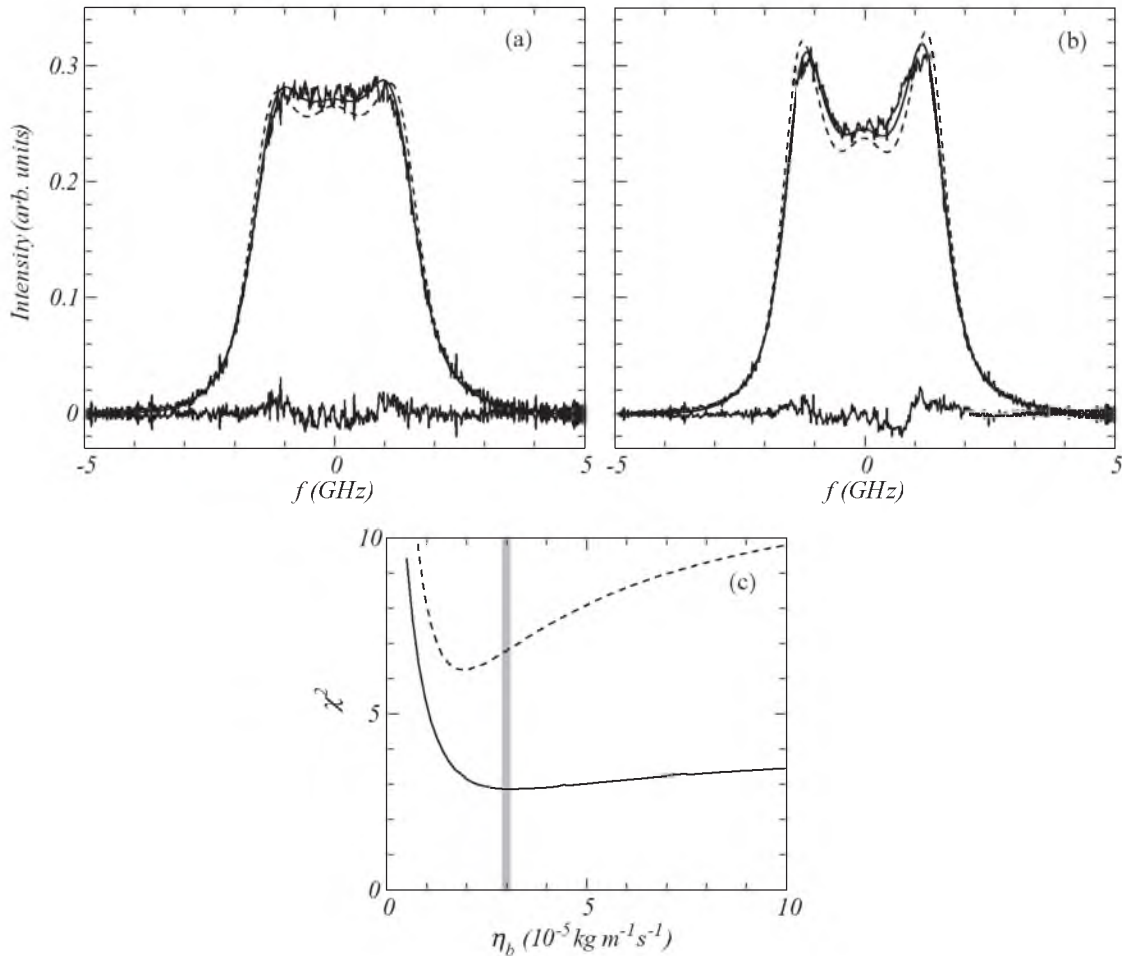

FIG. 8. O$_2$ coherent Rayleigh-Brillouin scattering for for $p = 2$ and 3 bar for (a) and (b), respectively. The dimensionless pressures are $y = 1.07$ and 1.61, respectively. Full lines show model spectra computed using the Tenti S6 model; dashed lines show model spectra using the Tenti S7 model. The model spectra were computed for $\eta_b = 3.0 \times 10^{-5}$ kg m^{-1} s^{-1}. Lower full line shows the difference between experiment and the Tenti S6 model. (c) χ^2 error as a function of η_b for $p = 3$ bar; the full line is using the S6 model, the dashed line is using the S7 model. The χ^2 error at $p = 3$ using the S6 model has a minimum at $\eta_b = 3.0 \times 10^{-5}$ kg m^{-1} s^{-1}; the value of η_b at smaller pressures cannot be determined in this way.

is much larger than that of the spontaneous Rayleigh-Brillouin experiments. Also, the mode structure of the pump laser can just be observed in the residue.

At these pressures, there is not a clear minimum of χ^2 versus η_b. Clear minima are found for higher pressures, where the influence of the bulk viscosity is stronger. From measurements at $p = 5$ bar, we infer a bulk viscosity $\eta_b = 2.6 \times 10^{-5}$ kg m^{-1} s^{-1}, with a statistical error of $\sigma_{\eta_b} = 0.5 \times 10^{-5}$ kg m^{-1} s^{-1} [35]. This value agrees with that found from spontaneous Rayleigh-Brillouin spectra, but is larger than the literature value of $\eta_b = 1.28 \times 10^{-5}$ kg m^{-1} s^{-1} [44]. Using the error analysis [Eq. (5)], we find that, for the coherent Rayleigh-Brillouin experiments, the statistical error in η_b is comparable to the systematic error.

In Fig. 8, we show coherent Rayleigh-Brillouin spectra for O$_2$ at pressures $p = 2$ and 3 bar. Similar to the N$_2$ spectra, the noise in the spectrum is relatively large. At $p = 3$ bar there is a shallow minimum of χ^2 versus η_b at $\eta_b = 3.0 \times 10^{-5}$ kg m^{-1} s^{-1}. From this shallow minimum we estimate a large statistical error $\sigma_{\eta_b} = 1.0 \times 10^{-5}$ kg m^{-1} s^{-1}. At $p = 5$ bar, a clear minimum gives $\sigma_{\eta_b} = 2.3 \pm 0.3 \times$

10^{-5} kg m^{-1} s^{-1}, which is significantly larger than the literature value, $\eta_b = 0.808 \times 10^{-5}$ kg m^{-1} s^{-1} [35].

Coherent Rayleigh-Brillouin scattering measurements on N$_2$ and O$_2$ for a range of pressures have previously been reported by Pan *et al.* and compared to the Tenti S7 model [24]. With the improved statistical accuracy of the present experiments, we conclude that the S6 model provides a significantly better fit of the spectra.

Due to the fluctuating mode structure of the pump laser, the fluctuations in coherent Rayleigh-Brillouin spectra are much larger than in the spontaneous spectra. However, the results of both experiments agree: the bulk viscosities of N$_2$ and O$_2$ gases are larger than their literature values, while in both cases the Tenti S6 model provides a better fit to the experiments than the S7 model. This is remarkable because the nature of the collective density fluctuations is very different in both experiments, leading to very different spectral line shapes.

C. Gas mixtures

Successful comparisons of the mixture model by Marquez *et al.* have been done for spontaneous Rayleigh-Brillouin
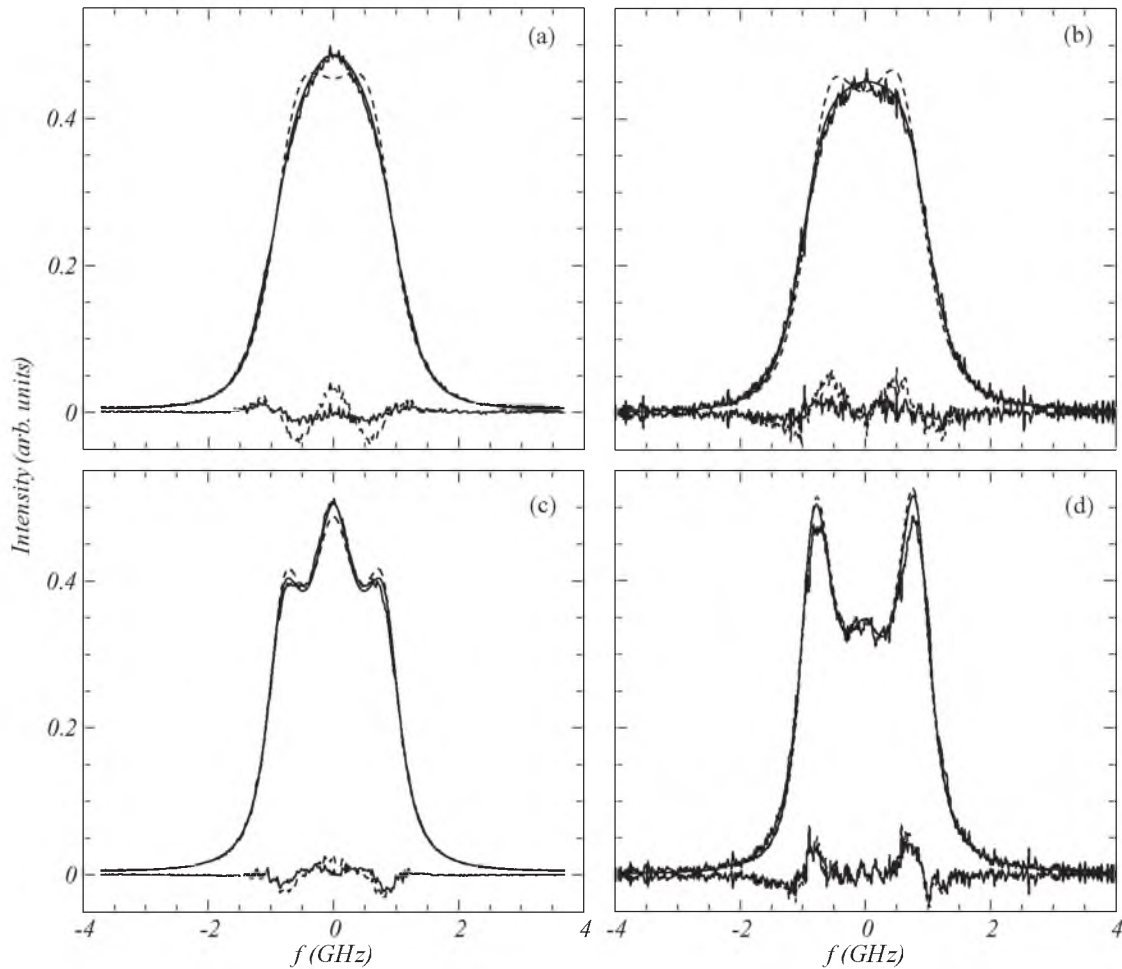

FIG. 9. Comparison of mixture models with for spontaneous Rayleigh-Brillouin scattering and coherent Rayleigh-Brillouin scattering on a gas of Kr atoms. (a) Spontaneous Rayleigh-Brillouin scattering, $p = 1$ bar ($y = 0.63$); (b) coherent Rayleigh-Brillouin scattering, $p = 1$ bar ($y = 0.67$); (c) spontaneous Rayleigh-Brillouin scattering, $p = 3$ bar ($y = 2.05$); (d) coherent Rayleigh-Brillouin scattering, $p = 3$ bar ($y = 1.86$). Full lines show the Tenti S6 model, dashed lines show the mixture model. Lower full line shows the difference between experiment and the Tenti S6 model; lower dashed line shows the difference between experiment and the mixture model.
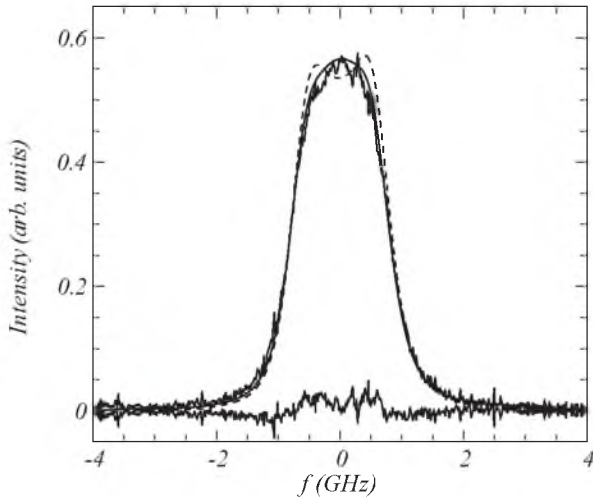
FIG. 10. Coherent Rayleigh-Brillouin scattering on an equimolar mixture of He and Xe (1 bar He and 1 bar Xe) at $p = 2$ bar (dimensionless pressure $y = 1.18$). Full line shows a prediction of the mixture model by Marquez [8]; dashed line shows a mixture model computed for a single gas of Xe atoms at $p = 1$ bar. Lower full line shows the difference between experiment and the mixture model.

scattering on mixtures of noble gases at relatively high pressures [7] (3.8–6 atm), and for coherent Rayleigh-Brillouin scattering on Ar and Kr with the lowest pressure $p = 1.5$ atm [8]. In order to test the accuracy of the model for a single noble gas, we first show spontaneous and coherent spectra on Kr in Fig. 9. For both cases, the deviation between model and experiment at 1 bar is relatively large. This result suggests that interactions other than hard-sphere interactions should be considered in the model.

Coherent spectra in an equimolar mixture of He and Xe at 2 bar are shown in Fig. 10 and compared to the mixture model [8]. In order to illustrate the influence of the helium

in the mixture, we also compare the measured spectrum to a single gas of Xe at 1 bar.

In the coherent arrangement, the polarizability of an atom determines both the force in the standing electric field and the scattered light intensity. Therefore, the coherent Rayleigh-Brillouin scattering signal of a mixture depends quadratically on the polarizability α of the atoms. As α of Xe is a factor 20 larger than that of He, the relaxation of sound is predominantly probed by the Xe atoms. Figure 10 illustrates that the model compares well to the experiment, and predicts a line shape that is very different from scattering on a single Xe gas at the same partial pressure.

As Fig. 9 illustrates, the hard-sphere model considered here does not predict the line shapes well at low pressures. Therefore, the successful prediction of the He-Xe mixture results in Fig. 10 might be fortuitous. In any case, the model predicts the large influence of the spectator atom (He) on the mixture line shape.

To illustrate the influence of He on the coherent Rayleigh-Brillouin spectrum of CO_2, we show in Fig. 11(a) the line shape of an equimolar mixture of He and CO_2 at $p = 2$ bar, and compare it to a spectrum of pure CO_2 at $p = 1$ bar in Fig. 11(b). Whilst the last spectrum can be modelled well by the Tenti S6 model, it significantly differs from the mixture experiment.

VIII. CONCLUSION

The Tenti S6 model reproduces Rayleigh-Brillouin spectra of single molecular gases remarkably well. However, a reconsideration of the value of the bulk viscosity was needed. This is legitimate because η_b has, so far, been determined in acoustic experiments at frequencies that are several orders of magnitude smaller than the GHz frequencies of light scattering experiments.

It is possible that, with our precise spontaneous Rayleigh-Brillouin experiments, we start to see the limits of the Tenti S6 model. This is also suggested by the pressure dependence of η_b in O_2 in Fig. 5. Since the pressure determines the value of
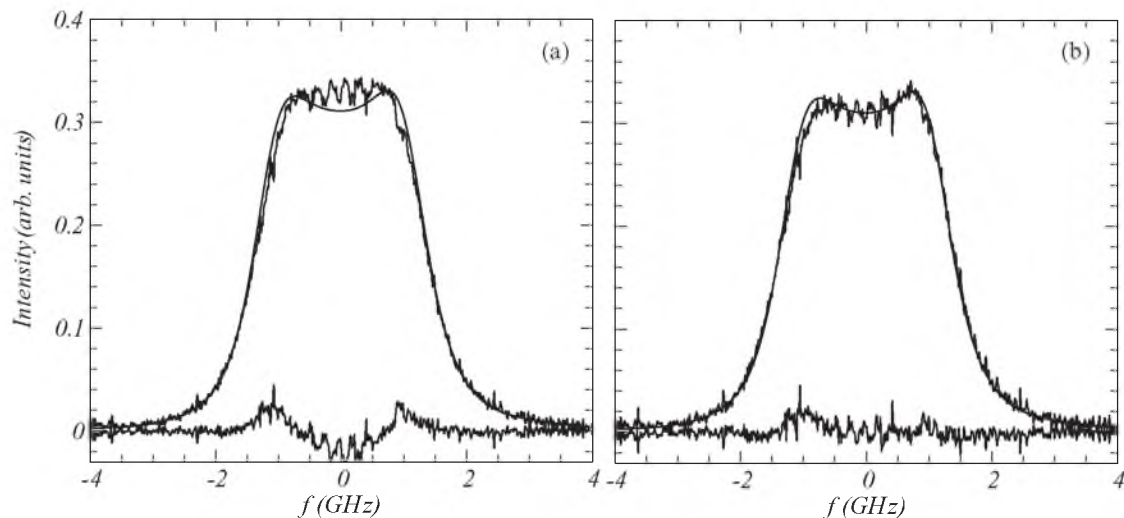

FIG. 11. (a) Coherent Rayleigh-Brillouin scattering on an equimolar mixture of He and CO_2 at $p = 2$ bar, (b) on pure CO_2 at $p = 1$ bar. Full lines show the prediction of the Tenti S6 model, using $\eta_b = 0.4 \times 10^{-5}$ kg m^{-1} s^{-1}. The difference between the measurement and the Tenti S6 model is shown at the bottom. The presence of He significantly affects the spectrum of the He-CO_2 mixture.

the y parameter, which is also the dimensionless wavelength, this may point to a wavelength dependence of η_b, which may arise if the relaxation of a density perturbation is also due to the diffusion of excited molecules [47].

Using coherent Rayleigh-Brillouin scattering, Pan *et al.* found that the bulk viscosity of CO_2 at sound frequencies corresponding to optical wavelengths was much smaller than what was known from acoustical experiments [48–50], which shows that that, while vibration modes are thermally accessible in CO_2, their relaxation rate is slow with respect to the GHz frequencies of light scattering experiments. Therefore, while vibration modes may partake in the bulk viscosity at ultrasound frequencies, they remain frozen in light scattering experiments. Surprisingly, for N_2 and O_2 molecules we find a larger η_b. Clearly, the argument involving vibrational degrees of freedom does not apply here since the lowest vibrational levels are orders of magnitude above $k_B T$ at room temperature, and there should be no reason not to use the literature values of η_b which were determined at ultrasound frequencies.

In our coherent Rayleigh-Brillouin scattering experiments, the statistical accuracy is compromised by the random mode fluctuations of the pump laser, which induces the density waves. Still, these experiments lead to the same conclusion regarding the value of η_b and the superiority of the S6 model.

We have also made a first step in testing a recent model [8] for coherent Rayleigh-Brillouin scattering experiments in mixtures of gases. Surprisingly, in mixtures of He and Xe atoms, and of He and CO_2 molecules, the He atoms hardly partake in the density waves and hardly contribute to the scattered light signal, but they clearly influence the Brillouin spectral line shapes of these mixtures. Because the hard-sphere model that underlies the mixture models in [7,8] does not appear adequate for noble gases at low pressures, and because it cannot represent molecules with internal degrees of freedom, there is a clear need to design line-shape models for mixtures of molecules along the lines of [7,8]. We hope that our experiments inspire further development of such models.

ACKNOWLEDGMENTS

[1] J. W. Strutt (Lord Rayleigh), Philos. Mag. **47**, 375 (1899).

[2] R. J. Strutt, Proc. R. Soc. London **95**, 155 (1918).

[3] C. Raman and K. Krishnan, Nature (London) **121**, 501 (1928).

[4] C. D. Boley, R. C. Desai, and G. Tenti, Can. J. Phys. **50**, 2158 (1972).

[5] G. Tenti, C. D. Boley, and R. C. Desai, Can. J. Phys. **52**, 285 (1974).

[6] *ESA's Report to the 37th Cospar Meeting—July 2008, Montreal, Canada, July 2008*, edited by K. Fletcher (ISBN 9789292214043).

[7] J. R. Bonatto and W. Marquez Jr., J. Stat. Mech. (2005) P09014.

[8] W. Marquez Jr., J. Stat. Mech. (2007) P03013.

[9] T. J. Greytak and G. B. Benedek, Phys. Rev. Lett. **17**, 179 (1966).

[10] E. H. Hara, A. D. May, and H. P. F. Knaap, Can. J. Phys. **49**, 420 (1971).

[11] R. P. Sandoval and R. L. Armstrong, Phys. Rev. A **13**, 752 (1976).

[12] A. Sugawara and S. Yip, Phys. Fluids **10**, 1911 (1976).

[13] Q. H. Lao, P. E. Schoen, and B. Chu, J. Chem. Phys. **64**, 3547 (1976).

[14] Q. H. Lao, P. E. Schoen, and B. Chu, Rev. Sci. Instrum. **47**, 418 (1976).

[15] X. Pan, M. N. Shneider, and R. B. Miles, Phys. Rev. A **71**, 045801 (2005).

[16] V. Ghaem-Maghami and A. D. May, Phys. Rev. A **22**, 692 (1980).

[17] V. Ghaem-Maghami and A. D. May, Phys. Rev. A **22**, 698 (1980).

[18] L. Letamendia, J. P. Chabrat, G. Nouchi, J. Rouch, C. Vaucamps, and S. H. Chen, Phys. Rev. A **24**, 1574 (1981).

[19] L. Letamendia, P. Joubert, J. P. Chabrat, J. Rouch, C. Vaucamps, C. D. Boley, S. Yip, and S. H. Chen, Phys. Rev. A **25**, 481 (1982).

[20] C. Y. She, G. C. Herring, H. Moosmüller, and S. A. Lee, Phys. Rev. Lett. **51**, 1648 (1983).

[21] C. Y. She, G. C. Herring, H. Moosmüller, and S. A. Lee, Phys. Rev. A **31**, 3733 (1985).

[22] J. H. Grinstead and P. F. Barker, Phys. Rev. Lett. **85**, 1222 (2000).

[23] X. Pan, M. N. Shneider, and R. B. Miles, Phys. Rev. Lett. **89**, 183001 (2002).

[24] X. Pan, M. N. Shneider, and R. B. Miles, Phys. Rev. A **69**, 033814 (2004).

[25] X. Pan, P. F. Barker, A. Meschanov, J. H. Grinstead, M. N. Shneider, and R. B. Miles, Opt. Lett. **27**, 161 (2002).

[26] H. T. Bookey, A. I. Bishop, and P. F. Barker, Opt. Express **14**, 3461 (2006).

[27] G. Dong, W. Lu, and P. F. Barker, Phys. Rev. A **69**, 013409 (2004).

[28] P. F. Barker and M. N. Shneider, Phys. Rev. A **64**, 033408 (2001).

[29] M. N. Shneider, P. F. Barker, X. Pan, and R. B. Miles, Opt. Commun. **239**, 205 (2004).

[30] H. T. Bookey, M. N. Shneider, and P. F. Barker, Phys. Rev. Lett. **99**, 133001 (2007).

[31] A. Chapman and T. G. Cowling, *Mathematical Theory of Non-uniform Gases*, 3rd ed. (Cambridge University Press, Cambridge, 1970).

[32] B. Witschas, M. O. Vieitez, E.-J. van Duijn, O. Reitebuch, W. van de Water, and W. Ubachs, Appl. Opt. **49**, 4217 (2010).

[33] G. Batchelor, *An Introduction to Fluid Dynamics*, 19th ed. (Cambridge University Press, Cambridge, 1967).

[34] K. E. Herzfeld and T. A. Litoviz, *Absorption and Dispersion of Ultrasonic Waves* (Academic Press, London, 1959).

[35] A. S. Meijer, A. S. de Wijn, M. Peters, N. Dam, and W. van de Water, to appear in J. Chem. Phys. (2010).

[36] W. E. Meador, G. A. Milner, and L. W. Townsend, Phys. Fluids **8**, 258 (1996).

[37] X. Pan, M. N. Shneider, and R. B. Miles, Phys. Rev. A **69**, 033814 (2004).

[38] H. Bookey, A. Bishop, M. N. Shneider, and P. Barker, J. Raman Spectrosc. **37**, 655 (2006).

[39] H. T. Bookey, M. N. Shneider, and P. F. Barker, Phys. Rev. Lett. **99**, 133001 (2007).

[40] L. Westling, M. Raymer, and J. Snyder, J. Opt. Soc. Am. B **1**, 150 (1984).

[41] P. Langenbeck, Appl. Opt. **9**, 2053 (1970).

[42] J. R. Rogers, J. Opt. Soc. Am **72**, 638 (1982).

[43] T. T. Kajava, H. M. Lauranto, and A. T. Friberg, J. Opt. Soc. Am. A **11**, 2045 (1994).

[44] G. J. Prangsma, A. H. Alberga, and J. J. J. Beenakker, Physica **64**, 278 (1973).

[45] P. Thompson, *Compressible-Fluid Dynamics* (McGraw-Hill, New York, 1972).

[46] N. A. Clark, G. R. Mellman, and T. J. Greytak, Phys. Rev. Lett. **29**, 150 (1972).

[47] M. Weinberg, R. Kapral, and R. C. Desai, Phys. Rev. A **7**, 1413 (1973).

[48] J. Xu, X. Ren, W. Gong, R. Dai, and D. Liu, Appl. Opt. **42**, 6704 (2003).

[49] X. Pan, M. N. Shneider, Z. Zhang, and R. B. Miles, *The 42nd Aerospace Sciences Meeting and Exhibit Conference* (2004), Vol. AIAA-2004-0017, p. 1.

[50] X. Pan, M. N. Shneider, and R. B. Miles, Phys. Rev. A **71**, 045801 (2005).